

Article

# Spin Crossover in Three Mononuclear Iron (III) Schiff Base Complexes

Ivan Nemeč<sup>1,2,\*</sup> , Ingrid Svoboda<sup>3</sup> and Radovan Herchel<sup>1</sup> 

<sup>1</sup> Department of Inorganic Chemistry, Faculty of Science, Palacký University, 17. listopadu 1192/12, 771 46 Olomouc, Czech Republic

<sup>2</sup> Central European Institute of Technology, CEITEC BUT, Technická 3058/10, 61600 Brno, Czech Republic

<sup>3</sup> Material sciences, Darmstadt University of Technology, D-64287 Darmstadt, Germany

\* Correspondence: ivan.nemec@upol.cz; Tel.: +420-585-634-354

Received: 10 July 2019; Accepted: 31 July 2019; Published: 2 August 2019



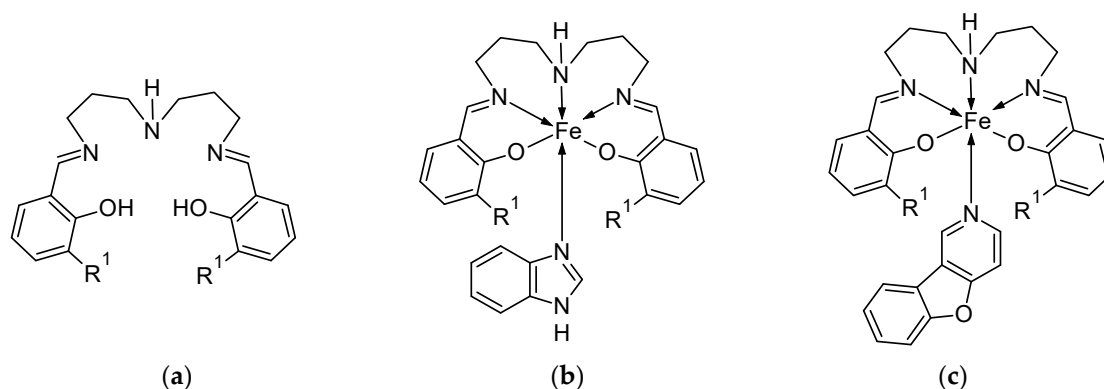
**Abstract:** The synthesis, crystal structure, and magnetic properties of three new mononuclear complexes  $[\text{Fe}(\text{R-LA})(\text{L1})](\text{BPh}_4)$ , where  $\text{R-LA}^{2-}$  is a doubly deprotonated pentadentate Schiff base ligand and L1 is a monodentate benzimidazole or furopyridine ligand, are reported. Ligand- and anion-driven changes in crystal structures and magnetic behavior were investigated in terms of the magnetic susceptibility measurements and theoretical calculations.

**Keywords:** spin crossover; Schiff base ligands; iron (III) complex; structure; magnetism

## 1. Introduction

Spin crossover (SCO) of (pseudo)octahedral complexes of iron(III) manifests as spin transition between  $S = 1/2$  (low-spin, LS) and  $S = 5/2$  (high-spin, HS) states [1]. Typically, the iron(III) complexes exhibit SCO for several types of coordination environments such as  $\{\text{FeO}_6\}$ ,  $\{\text{FeO}_3\text{S}_3\}$ ,  $\{\text{FeS}_6\}$ ,  $\{\text{FeN}_2\text{O}_2\text{S}_2\}$ ,  $\{\text{FeN}_3\text{O}_3\}$ , or  $\{\text{FeN}_6\}$ , but the most explored are the  $\{\text{FeN}_4\text{O}_2\}$  complexes with tri-, tetra-, penta-, or hexadentate Schiff base ligands [2]. For the last decade our attention focused predominantly on the Fe(III) complexes with pentadentate Schiff bases originating from reactions between derivatives of various ortho-hydroxy salicylaldehydes and aliphatic triamines [3–7]. In these compounds, two basic types of SCO complexes can be recognized due to different kinds of amine used in the synthesis of Schiff base ligands: so-called symmetric ones in which derivatives of bis(3-aminopropyl)amine are used ( $\text{H}_2\text{R-LA}$ , R-substituted compounds of 4-azaheptamethylene-1,7-bis(salicylideneimine),  $\text{H}_2\text{LA}$ ) and asymmetric ones with *N*-(2-aminoethyl)-1,3-propanediamine ( $\text{H}_2\text{R-LB}$ , R-substituted compounds of 4-azahexamethylene-1,7-bis(salicylideneimine),  $\text{H}_2\text{LB}$  Scheme 1). Initially, SCO was observed only for compounds with the general formula  $[\text{Fe}(\text{R-LA})(\text{L1})](\text{BPh}_4)$  [8] or  $[\{\text{Fe}(\text{R-LA})\}_2(\mu\text{-L2})](\text{BPh}_4)$  [9], and the observed transitions were of gradual or even spin equilibrium character. One exception was found in the case of a mononuclear compound with  $\text{R-LA} = \text{bis}(3\text{-methoxysalicylideneiminopropyl})\text{methylamine}$  and  $\text{L1} = 4\text{-aminopyridine}$ , which exhibited rather cooperative SCO, possibly due to its crystal packing involving  $\text{N-H}\cdots\text{O}$  and  $\text{N-H}\cdots\pi$  non-covalent interactions between the complex cations [10]. Other interesting results were obtained for compounds  $[\text{Fe}(\text{LA})(\text{L1A})][\text{M}(\text{dmit})_2]\cdot\text{CH}_3\text{CN}$ ,  $\text{M} = \text{Ni}, \text{Pd}, \text{Pt}$ , in which L1A (1-(pyridin-4-yl)-2-(*N*-methylpyrrol-2-yl) ethane) is a photoisomerable ligand and  $[\text{M}(\text{dmit})_2]^-$  anions can act as molecular conductors [11]. Compounds of the general formula  $[\text{Fe}(\text{LA})(\text{L1B})](\text{BPh}_4)$  also contain photoisomerable ligands L1B = 3-phenylazopyridine or 4-phenylazopyridine [12]. Nevertheless, these complexes are not very interesting from a magnetic point of view because they exhibit only gradual spin transitions. This changed with the introduction of the shorter aliphatic chain in Schiff base ligands by substitution of the derivatives of bis(3-aminopropyl)amine by *N*-(2-aminoethyl)-1,3-propanediamine. Increased rigidity of the resulting

ligands (supported also by the introduction of naphthyl instead of benzene rings) led to preparation of the  $[\text{Fe}(\text{LB})(\text{LP})]$  complexes (where LP stands for (1) pseudohalido ligand), which exhibited cooperative spin transitions, in some cases even accompanied by thermal hysteresis [3].



**Scheme 1.** Structural formulas of (a) ligands  $\text{H}_2\text{LA}$  ( $\text{R}^1 = \text{H}$ ) and  $\text{H}_23\text{EtO-LA}$  ( $\text{R}^1 = \text{O-CH}_2\text{-CH}_3$ ) and (b) complex cations  $[\text{Fe}(3\text{EtO-LA})(\text{L}^{1\text{a}})]^+$  in **1a** ( $\text{R}^1 = \text{O-CH}_2\text{-CH}_3$ ) and (c)  $[\text{Fe}(3\text{EtO-LA})(\text{L}^{1\text{b}})]^+$  in **2a** ( $\text{R}^1 = \text{O-CH}_2\text{-CH}_3$ ) or  $[\text{Fe}(\text{LA})(\text{L}^{1\text{b}})]^+$  in **2b** ( $\text{R}^1 = \text{H}$ ).

Inspired by the abovementioned results we decided to attempt preparation of the  $[\text{Fe}(\text{LA})(\text{L}^1)](\text{BPh}_4)$  complexes exhibiting cooperative SCO by using monodentate ligands, which could increase the rigidity and the number of significant non-covalent interactions in the resulting complexes. Therefore, we decided to use two different bulky monodentate ligands, benzimidazole ( $\text{L}^{1\text{a}}$ ) and 1-benzofuro[3,2-c]pyridine ( $\text{L}^{1\text{b}}$ ), together with two slightly different pentadentate ligands,  $\text{H}_2\text{LA}$  and  $\text{H}_23\text{EtO-LA}$  (4-azaheptamethylene-1,7-bis(3-thoxy-salicylideneimine), Scheme 1). We were successful in the preparation of three compounds:  $[\text{Fe}(3\text{EtO-LA})(\text{L}^{1\text{a}})](\text{BPh}_4)$  (**1a**),  $[\text{Fe}(3\text{EtO-LA})(\text{L}^{1\text{b}})](\text{BPh}_4)\cdot\text{CH}_3\text{OH}$  (**2a**), and  $[\text{Fe}(\text{LA})(\text{L}^{1\text{b}})](\text{BPh}_4)$  (**2b**). Here, we report their crystal structure and magnetic properties.

## 2. Materials and Methods

Chemicals were purchased from commercial sources (Sigma-Aldrich) and used as received. 1-benzofuro[3,2-c]pyridine was prepared according to a previously reported procedure [13,14]. Elemental analysis was carried out on a Flash 2000 (ThermoFisher Scientific, Waltham, MA, USA).

Magnetic susceptibility and magnetization measurements were done using a SQUID magnetometer (Quantum Design Inc., San Diego, CA, USA) from  $T = 2$  K at  $B = 0.1$  T. The magnetization data were taken at  $T = 2.0$  and 4.6 K, respectively. Raw susceptibility was corrected, and diamagnetic corrections of the constituent atoms were estimated from Pascal constants. The effective magnetic moment was calculated as usual:  $\mu_{\text{eff}}/\mu_{\text{B}} = 798(\chi''T)^{1/2}$  when SI units are employed.

Single-crystal X-ray diffraction data were collected on an Oxford diffractometer Xcalibur2 (Oxford Diffraction Ltd., Oxford, UK) with a Sapphire CCD detector and fine-focused sealed tube (Mo  $K\alpha$  radiation,  $\lambda = 0.71073$  Å) source and equipped with an Oxford Cryosystem nitrogen gas-flow apparatus. All structures were solved and refined (full-matrix least-squares on  $F_o^2 - F_c^2$ ) by using SHELXS2014 software [15].

### 2.1. Synthesis

#### 2.1.1. Ligands

Neutral, pentadentate ligands  $\text{H}_2\text{LA}$  and  $\text{H}_23\text{EtO-LA}$  were prepared by mixing the appropriate aldehyde and amine in a 2:1 molar ratio. Synthesis of all Schiff base ligands is analogous; therefore, only synthesis of  $\text{H}_2\text{LA}$  is presented in detail [9]. A methanol solution of salicylaldehyde (2.44 g,

20 mmol in 50 cm<sup>3</sup>) was combined with di(3-aminopropyl)amine (1.31 g, 10 mmol) and the mixture was refluxed for 60 min. The ligand was obtained as a yellow solution ready for subsequent use.

### 2.1.2. Mononuclear Precursors

Synthesis of all precursors was very similar [9]; therefore, only the synthesis of [Fe(LA)Cl] is described. The methanol solution of ligand H<sub>2</sub>LA (10 mmol in 50 cm<sup>3</sup>) was combined with a solution of iron(III) chloride hexahydrate (2.70 g, 10 mmol) in 40 cm<sup>3</sup> of methanol. The mixture was refluxed for 20 min, and then triethylamine (2.22 g, 22 mmol) was added to complete deprotonation of the Schiff base ligand. The resulting violet solution was refluxed for 30 min and left to cool slowly to room temperature when a dark violet micro-crystalline powder precipitated. This was filtered off using a fritted funnel, washed with methanol and diethylether, and dried.

### 2.1.3. Mononuclear Complexes **1a**, **2a**, and **2b**

The complexes were prepared in the same manner by mixing 100 mg of the [Fe(LA)Cl] or [Fe(3EtO-LA)Cl] (0.193 mmol in the preparation of **1a** and **2a**, 0.233 mmol in the preparation of **2b**) precursor complexes with a heterocyclic derivate (23 mg of L1<sup>a</sup> for the preparation of **1a**, 33/38 mg of L1<sup>b</sup> for the preparation of **2a/2b**) in a molar ratio of 1:1. After 30 min of reflux, the solution was filtered through paper filter into an equimolar amount of solution of NaBPh<sub>4</sub>.

As an example, the synthesis of [Fe(3EtO-LA)(L1<sup>a</sup>)](BPh<sub>4</sub>) is described in detail. To a solution of [Fe(3EtO-LA)Cl] (100 mg in 30 cm<sup>3</sup> of methanol), L1<sup>a</sup> was added. The resulting violet solution was refluxed for 30 min and filtered into a solution of NaBPh<sub>4</sub> (66 mg in 5 cm<sup>3</sup>). Black crystals precipitated overnight. They were collected, washed with methanol and diethyl ether, and dried.

### 2.1.4. Elemental Analysis

**1a**: calcd (%) for C<sub>55</sub>B<sub>1</sub>Fe<sub>1</sub>H<sub>57</sub>N<sub>5</sub>O<sub>4</sub>, M<sub>w</sub> = 918.7 g·mol<sup>-1</sup>, C, 71.9; H, 6.3; N, 7.6. Found: C, 71.5; H, 6.1; N, 7.3. Yield = 67%.

**2a**: calcd (%) for C<sub>60</sub>B<sub>1</sub>Fe<sub>1</sub>H<sub>62</sub>N<sub>4</sub>O<sub>6</sub>, M<sub>w</sub> = 1001.8 g·mol<sup>-1</sup>, C, 71.9; H, 6.2; N, 5.6. Found: C, 71.6; H, 6.0; N, 5.2. Yield = 48%.

**2b**: calcd (%) for C<sub>55</sub>B<sub>1</sub>Fe<sub>1</sub>H<sub>50</sub>N<sub>4</sub>O<sub>3</sub>, M<sub>w</sub> = 881.7 g·mol<sup>-1</sup>, C, 74.9; H, 5.7; N, 6.4. Found: C, 74.5; H, 5.8; N, 6.1. Yield = 55%.

## 2.2. Theoretical Calculations

The theoretical calculations were carried out using the ORCA 4.1 computational package [16]. Three density functional theory (DFT) functionals, B3LYP [17–19], OPBE [20,21], and TPSSh [22,23], were used to optimize the molecular structures together with the polarized triple- $\zeta$  quality basis set def2-TZVP proposed by Ahlrichs and co-workers [24], where “verytightopt” optimization criteria were used in ORCA. The calculations utilized the RI approximation with the decontracted auxiliary def2/J Coulomb fitting basis set [25] and the chain-of-spheres (RIJCOSX) approximation to exact exchange [26,27] as implemented in ORCA. Increased integration grids (Grid5 and Gridx5 in ORCA convention) and tight SCF convergence criteria were used in all calculations. Moreover, the SCF stability test as implemented in ORCA was done for all final optimized geometries to verify whether the SCF solution was at a local minimum and not in a saddle point [28,29].

## 3. Results and Discussion

### 3.1. Crystal Structures

The crystal structures were determined by single-crystal X-ray diffraction for all three presented compounds **1a**, **2a**, and **2b**, and these crystallized in triclinic (*P*-1 for **1a** and **2a**) and monoclinic (*P*2<sub>1</sub>/*c* for **2b**) space groups (Table 1). All three compounds consist of complex Fe(III) cations charge balanced by BPh<sub>4</sub><sup>-</sup> anions. In **2a**, the additional methanol molecule is in its asymmetric unit, which is heavily

disordered. It was not possible to model it reasonably; therefore, the SQUEEZE procedure [30] was used to subtract the corresponding electronic density.

**Table 1.** Crystal data and details of structure determination.

Compound	1a	2a	2b
Formula	C <sub>55</sub> H <sub>57</sub> BFeN <sub>5</sub> O <sub>4</sub>	C <sub>59</sub> H <sub>58</sub> BFeN <sub>4</sub> O <sub>5</sub>	C <sub>55</sub> H <sub>50</sub> BFeN <sub>4</sub> O <sub>3</sub>
Formula weight	918.71	969.75	881.65
Crystal system	Triclinic	Triclinic	Monoclinic
Space group	<i>P</i> -1	<i>P</i> -1	<i>P</i> 2 <sub>1</sub> / <i>c</i>
Cell parameters			
<i>a</i> /Å	10.1648(7)	13.2869(4)	19.1978(10)
<i>b</i> /Å	15.2130(10)	13.6926(5)	11.7562(13)
<i>c</i> /Å	16.2320(10)	16.4083(6)	21.381(2)
$\alpha$ /°	81.990(6)	70.732(3)	90
$\beta$ /°	72.359(6)	78.232(3)	110.458(8)
$\gamma$ /°	86.049(6)	67.395(3)	90
<i>V</i> /Å <sup>3</sup>	2367.7(3)	2591.29(17)	4521.2(8)
<i>Z</i>	2	2	4
<i>T</i> /K	100(2)	190(2)	293(2)
Density, <i>D</i> <sub>c</sub> /g cm <sup>-3</sup>	1.289	1.243	1.295
Abs. coefficient/mm <sup>-1</sup>	0.371	0.344	0.384
Data/restraints/param	8326/0/601	6630/3/644	7931/0/577
R <sub>1</sub> <sup>a</sup> , wR <sub>2</sub> <sup>b</sup> (all data)	0.0660, 0.1073	0.0545, 0.0867	0.0618, 0.0810
R <sub>1</sub> <sup>a</sup> , wR <sub>2</sub> <sup>b</sup> [ <i>I</i> > 2σ( <i>I</i> )]	0.0379, 0.0978	0.0355, 0.0829	0.0340, 0.0763
Goodness of fit	1.049	1.028	0.954
CSD number	1939657	1939658	1939656

$$^a R_1 = \sum (|F_o| - |F_c|) / \sum |F_o|. \quad ^b wR_2 = \{ \sum [w(F_o^2 - F_c^2)^2] / \sum [w(F_o^2)^2] \}^{1/2}.$$

The complex cations in **1a**, **2a**, and **2b** consist of a pentadentate Schiff base ligand (3EtO-LA<sup>2-</sup> in **1a** and **2a**, LA<sup>2-</sup> in **2b**) coordinated to the central Fe(III) atom, and the sixth coordination site is occupied by a monodentate N-donor heterocyclic ligand (L1<sup>b</sup> in **2a** and **2b**, L1<sup>b</sup> in **1a**). The pentadentate Schiff base ligands coordinate iron centers in a *cis*-conformation of the oxygen atoms, which is typical for compounds with [Fe(R-LA)]<sup>+</sup> cations (Figure 1) [31]. The monodentate ligand is in a *trans*-position to the secondary amine group of the pentadentate ligand.

The metal–ligand bond lengths (Figure 1) are close to the values typical for the LS state with the longest bonds observed between the iron atoms and secondary nitrogen atoms of the pentadentate ligands (in Å, 2.0293(19) in **1a**, 2.0539(16) in **2a**, 2.0843(15) in **2b**) or the nitrogen atom of the heterocyclic monodentate ligand (in Å, 2.0105(18) in **1a**, 2.0497(15) in **2a**, 2.0990(16) in **2b**). The Fe–N bonds involving the imino nitrogen atoms are rather shorter and similar for all three structures, ranging between 1.98 to 2.01 Å. The Fe–O bonds are even shorter: 1.87–1.89 Å. The angular distortion parameter Σ is rather small [32]: 17.4° (**1a**), 23.7° (**2a**), and 30.3° (**2b**).

The crystal structures of **1a**, **2a**, and **2b** do not contain hydrogen bonding of significant strength. In **1a**, the secondary amine group from the complex cation forms offset N–H⋯π non-covalent contact with the aromatic ring of the BPh<sub>4</sub><sup>-</sup> anion. The shortest N⋯C distance is 3.446(3) Å (Figure S1 in supplementary materials). The N–H group from benzimidazole also forms N–H⋯π interaction with the aromatic ring of the BPh<sub>4</sub><sup>-</sup> anion—the N⋯C<sub>g</sub> distance is 3.227(4) Å (where C<sub>g</sub> stands for the ring centroid).

In **2a**, the interaction between complex cations is provided by very offset ring–ring interactions with a shortest C⋯C distance of 3.192(3) Å. Other non-covalent interactions include weak C–H⋯O and C–H⋯π contacts (Figure S2).

In **2b**, the secondary amine group from the complex cation forms weakly offset N–H⋯π interaction with the aromatic ring of the BPh<sub>4</sub><sup>-</sup> anion (the shortest N⋯C distance is 3.713(3) Å). Other non-covalent interactions in **2b** are weak C–H⋯O and C–H⋯π contacts (Figure S3).

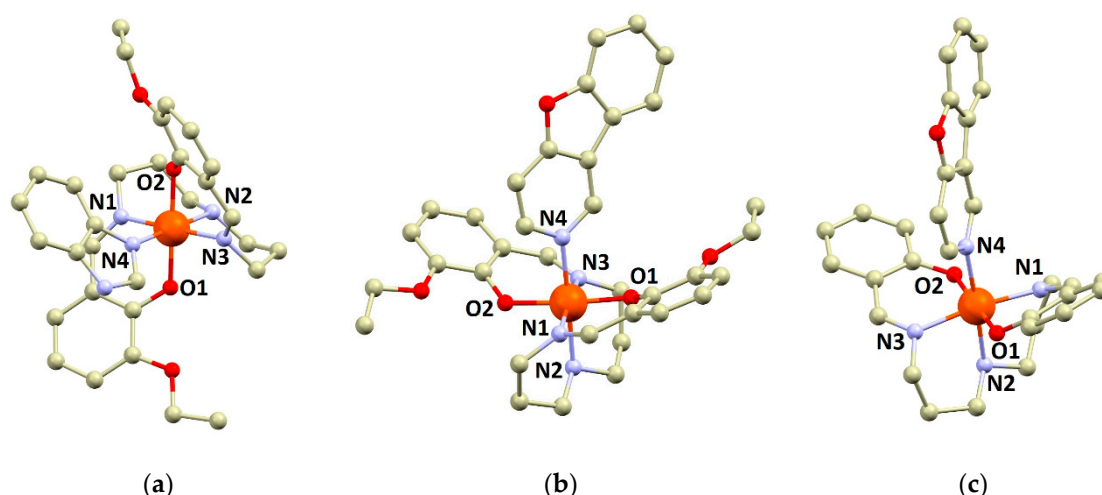


**Figure 1.** Depiction of the molecular structures of  $[\text{Fe}(3\text{EtO-LA})(\text{L1}^{\text{a}})]^+$  in **1a** (a),  $[\text{Fe}(3\text{EtO-LA})(\text{L1}^{\text{b}})]^+$  in **2a** (b) and  $[\text{Fe}(\text{LA})(\text{L1}^{\text{b}})]^+$  in **2b** (c). Selected bond lengths (in Å): in **1a**, Fe1–O1 = 1.8896(15), Fe1–O2 = 1.8951(15), Fe1–N1 = 1.9608(19), Fe1–N2 = 2.0293(19), Fe1–N3 = 1.971(2), Fe1–N4 = 2.0105(18); in **2a**, Fe1–O1 = 1.8719(12), Fe1–O2 = 1.8796(12), Fe1–N1 = 1.9787(15), Fe1–N2 = 2.0539(16), Fe1–N3 = 1.9840(15), Fe1–N4 = 2.0497(15); in **2b**, Fe1–O1 = 1.8885(13), Fe1–O2 = 1.8892(13), Fe1–N1 = 1.9997(17), Fe1–N2 = 2.0843(15), Fe1–N3 = 2.0099(16), Fe1–N4 = 2.0990(16).

### 3.2. Magnetic Properties

The temperature dependence of the effective magnetic moment for **1a**, **2a**, and **2b** is shown in Figure 2. All three compounds undergo spin crossover from the LS to the HS state ( $S = 1/2 \rightarrow 5/2$ ), which start above ca. 150 K. Evidently, the spin crossover is incomplete until 300 K, because room temperature values of the effective magnetic moment are less than the spin-only value for  $S = 5/2$  and  $g = 2.0$  ( $5.93 \mu_{\text{B}}$ ). Moreover, the low temperature values of  $\mu_{\text{eff}}$  vary in the range  $\approx 2\text{--}3 \mu_{\text{B}}$ , which suggests that a small portion of iron(III) complexes stay in the HS state. This is also supported by the field dependence of molar magnetization measurements (measured at 2 and 4.6 K, Figure S4), which unequivocally confirm the LS ground state with a larger contribution of non-converted HS molecules in **1a** and **2a** ( $M_{\text{mol}}/N_{\text{A}}\mu_{\text{B}} = 1.5$  in **1a**, 1.4 in **2a** at 2 K and 7 T) than in **2b** ( $M_{\text{mol}}/N_{\text{A}}\mu_{\text{B}} = 1.1$  at 2 K and 7 T).

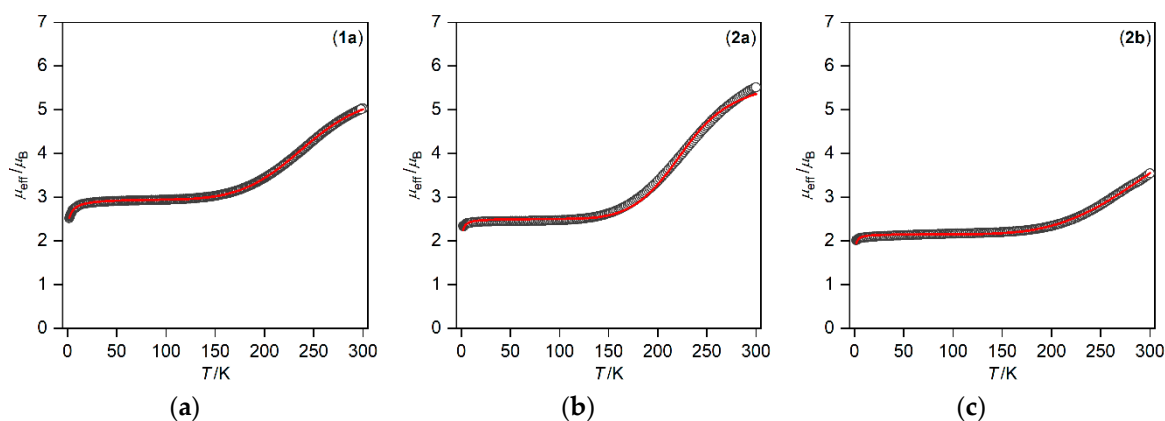


**Figure 2.** The temperature dependence of the effective magnetic moment for **1a** (a), **2a** (b), and **2b** (c). The experimental data are displayed as empty circles, calculated data are displayed as full lines.

The experimental data were analyzed with the help of the Ising-like model [33,34] having following Hamiltonian

$$\hat{H} = \frac{\Delta}{2} \hat{\sigma} - \gamma \langle \sigma \rangle \hat{\sigma} \quad (1)$$

where  $\sigma$  is fictitious spin with eigenvalues  $-1$  for LS and  $+1$  for HS states,  $\Delta$  is the energy difference between HS and LS states,  $\gamma$  stands for the cooperativeness of the system ( $\gamma > 0$ ), and  $\langle\sigma\rangle$  is the thermal average of the fictitious spin, which is calculated by solving the implicit equation

$$\langle\sigma\rangle = \frac{-1 + r_{\text{eff}} \exp[-(\Delta - 2\gamma\langle\sigma\rangle)/kT]}{+1 + r_{\text{eff}} \exp[-(\Delta - 2\gamma\langle\sigma\rangle)/kT]} \quad (2)$$

where  $r_{\text{eff}}$  is the effective degeneracy ratio of HS and LS states, and it incorporates both the spin and vibrational degeneracies of the respective spin states [35]. Then, the molar fraction of HS species,  $x'_{\text{HS}}$ , is computed as

$$x'_{\text{HS}} = \frac{1}{2}(1 + \langle\sigma\rangle). \quad (3)$$

In order to fit the experimental magnetic data, the overall susceptibility was calculated as

$$\chi_{\text{mol}} = (x''_{\text{HS}} + x_{\text{rHS}})\chi_{\text{HS}} + (1 - x''_{\text{HS}} - x_{\text{rHS}})\chi_{\text{LS}} \quad (4)$$

where  $x_{\text{rHS}}$  is the mole fraction of the residual high-spin state at low temperature,  $x''_{\text{HS}}$  is the rescaled high-spin fraction calculated from the Ising-like model as  $x''_{\text{HS}} = x'_{\text{HS}}(1 - x_{\text{rHS}})$ , and the molar susceptibility values for LS and HS states were calculated by the Curie–Weiss law as

$$\chi_{\text{LS}} = \frac{N_{\text{A}}\mu_0\mu_{\text{B}}^2 S_{\text{LS}}(S_{\text{LS}} + 1)}{3k} \frac{g_{\text{LS}}^2}{T - \Theta_{\text{LS}}} \quad (5)$$

$$\chi_{\text{HS}} = \frac{N_{\text{A}}\mu_0\mu_{\text{B}}^2 S_{\text{HS}}(S_{\text{HS}} + 1)}{3k} \frac{g_{\text{HS}}^2}{T - \Theta_{\text{HS}}}. \quad (6)$$

To summarize, the variation of Ising-like model parameters ( $\Delta$ ,  $\gamma$ ,  $\rho_{\varepsilon\phi\phi}$ ) leads to temperature variation of the HS mole fraction, which is subsequently utilized to calculate the temperature variation of the overall molar susceptibility and, hence, the effective magnetic moment. Due to the fact that the spin crossover is not finished until 300 K, the  $g_{\text{HS}}$  value was fixed to 2.0, which is a typical value for HS octahedral iron(III) complexes. Also, the Weiss constant of the HS state was set to zero, because the low temperature data are dominated by the LS fraction. Then, we are left with these additional free parameters:  $g_{\text{LS}}$ ,  $x_{\text{rHS}}$ , and  $\Theta_{\text{LS}}$ . Finally, a fitting procedure was applied to find the best parameters describing the experimental magnetic data, and the values of the parameters are listed in Table 2. The spin transition temperatures  $T_{1/2}$  are increasing in the following order: **2a** < **1a** < **2b**.

**Table 2.** The magnetic parameters for **1a**, **2a**, and **2b**<sup>a</sup>.

Compound	$g_{\text{LS}}$	$\Theta_{\text{LS}}$	$x_{\text{rHS}}$	$\Delta$ (K)	$\gamma$ (K)	$r_{\text{eff}}$	$\Delta H$ (J mol <sup>-1</sup> )	$\Delta S$ (J K <sup>-1</sup> mol <sup>-1</sup> )	$T_{1/2}$ (K)
<b>1a</b>	2.34	-4.3	0.15	930	116	35.0	7730	29.6	262
<b>2a</b>	2.01	-1.5	0.10	1200	95	150	9975	41.7	239
<b>2b</b>	2.01	-0.8	0.05	1033	127	17	8592	23.6	365

<sup>a</sup> the thermodynamic parameters were calculated as  $\Delta H = N_{\text{A}}\Delta$ ,  $\Delta S = R \ln r_{\text{eff}}$ , and  $T_{1/2} = \Delta H / \Delta S$ .

### 3.3. Theoretical Calculations

In order to evaluate the impact of various coordinated heterocyclic ligands on the spin crossover properties of pentacoordinate Schiff base iron(III) complexes, density functional theory (DFT) calculations were employed. Here, we tested three DFT functionals, B3LYP, OPBE, and TPSSH, which were selected by benchmark studies to be suitable functionals for the study of spin crossover phenomena [36–38]. The molecular geometries of the complex cations  $[\text{Fe}(\text{R-LA})(\text{L1})]^+$  of **1a**, **2a**, and **2b** were optimized for LS (doublet) and HS (sextet) states. Furthermore, we added another three analogous SCO complexes, namely, DAVCEJ, DETBEJ, and KISJUS, to address the robustness of this

theoretical approach. The respective donor–acceptor distances calculated with the TPSSh functional are summarized in Table 3; for other functionals, please see Tables S1 and S2. The experimental X-ray data are available for the low-spin state of **1a**, DAVCEJ, and KISJUS, whereas DAVCEJ01 is only available in a high-spin state structure because the reported room temperature X-ray data of DETBEJ and KISJUS01 correspond to incomplete spin transition at this temperature with respect to the magnetic data.

**Table 3.** The interatomic donor–acceptor distances for density functional theory (DFT)-optimized geometries of  $[\text{Fe}(\text{R-LA})(\text{L1})]^+$  of **1a**, **2a**, and **2b** and DAVCEJ, DETBEJ, and KISJUS using the TPSSh functional <sup>a</sup>.

Method	Compound	Fe–O	Fe–N <sub>im</sub>	Fe–N <sub>am</sub>	Fe–N <sub>hetero</sub>
X-ray analysis	<b>1a</b> (LS)	1.8896/1.8951	1.9608/1.971	2.0293	2.0105
	DAVCEJ (LS)	1.869/1.880	1.961/1.974	2.091	2.000
	DAVCEJ01 (HS)	1.908/1.920	2.072/2.096	2.257	2.146
	KISJUS (LS, 100 K)	1.863/1.880	1.946/1.954	2.023	1.982
TPSSh (LS)	<b>1a</b>	1.875/1.892	1.949/1.972	2.047	2.010
	<b>2a</b>	1.872/1.880	1.979/1.984	2.054	2.050
	<b>2b</b>	1.888/1.889	2.000/2.010	2.084	2.099
	DAVCEJ	1.875/1.890	1.953/1.968	2.105	2.008
	DETBEJ	1.872/1.899	1.953/1.978	2.044	2.016
	KISJUS	1.867/1.896	1.949/1.972	2.044	1.991
	TPSSh (HS)	<b>1a</b> (HS)	1.931/1.950	2.104/2.113	2.282
<b>2a</b> (HS)		1.934/1.936	2.105/2.109	2.281	2.229
<b>2b</b> (HS)		1.939/1.942	2.104/2.107	2.276	2.225
DAVCEJ (HS)		1.938/1.945	2.095/2.098	2.345	2.202
DETBEJ (HS)		1.938/1.939	2.105/2.109	2.276	2.228
KISJUS (HS)		1.935/1.945	2.107/2.109	2.286	2.174

<sup>a</sup> distances in Å.

Figure 3 shows a comparison of DFT-optimized donor–acceptor distances with the experimental data. It is evident that none of these DFT functionals provided perfect results: both B3LYP and OPBE overestimated Fe–N<sub>am</sub> and Fe–N<sub>het</sub> distances; Fe–N<sub>im</sub> was overestimated by B3LYP and underestimated by OPBE. Moreover, the Fe–N<sub>am</sub> distance of DAVCEJ (HS) is extremely long. It seems to us that the best results were provided by the TPSSh functional. Indeed, only this functional correctly predicted the LS ground state for the studied compounds according to the energy comparison of HS and LS isomers depicted in Figure 4. However, there is large variation in the energy difference,  $E_{\text{HS}}-E_{\text{LS}}$ , between 1.92 kcalmol<sup>-1</sup> for **2a** and 12.91 kcalmol<sup>-1</sup> for DETBEJ. Obviously, the  $E_{\text{HS}}-E_{\text{LS}}$  energy difference does not correlate with the  $T_{1/2}$  value of the studied compounds, and this inconsistency could also be ascribed to variation of the entropy within this series. However, all the studied compounds have a very similar composition of the Fe<sup>III</sup> complex cation and have BPh<sub>4</sub><sup>-</sup> as the counterion; thus, it can be anticipated that variation of the entropy for the whole series should be minute. Thus, it is most likely that the large variation in the  $E_{\text{HS}}-E_{\text{LS}}$  energy difference is due to imperfectness of the DFT functional and/or due to neglect of the crystal packing and non-covalent intermolecular interactions in the solid state, which cannot be reproduced with geometry optimization of  $[\text{Fe}(\text{R-LA})(\text{L1})]^+$  cations in vacuum.

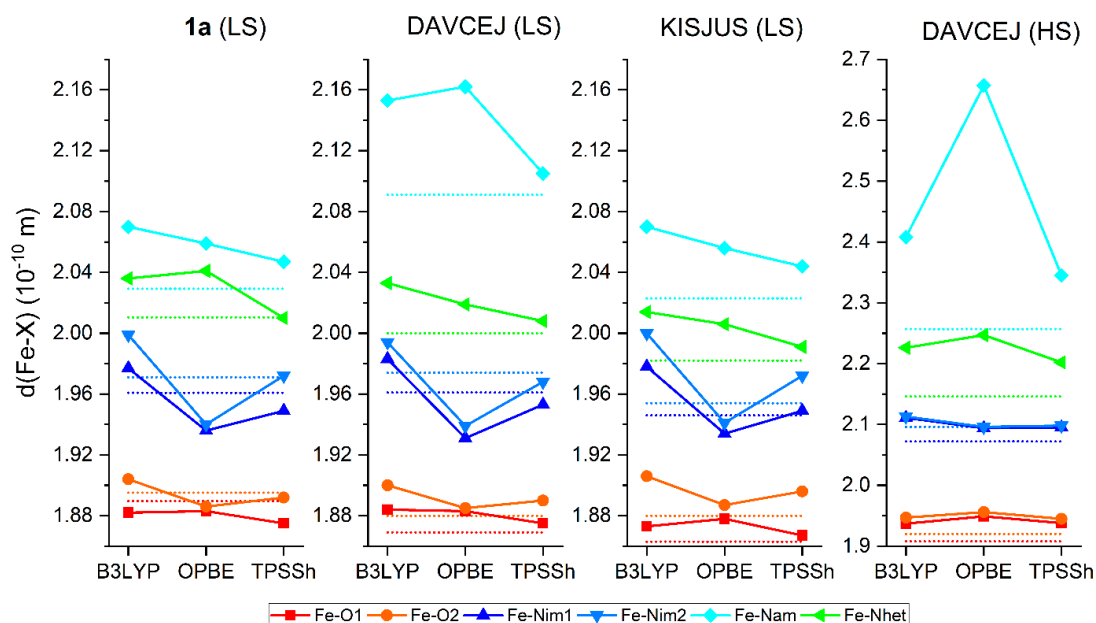


**Figure 3.** The variation of the donor–acceptor distances in DFT-optimized geometries (full lines + symbols) compared to the experimental X-ray data (dotted lines).

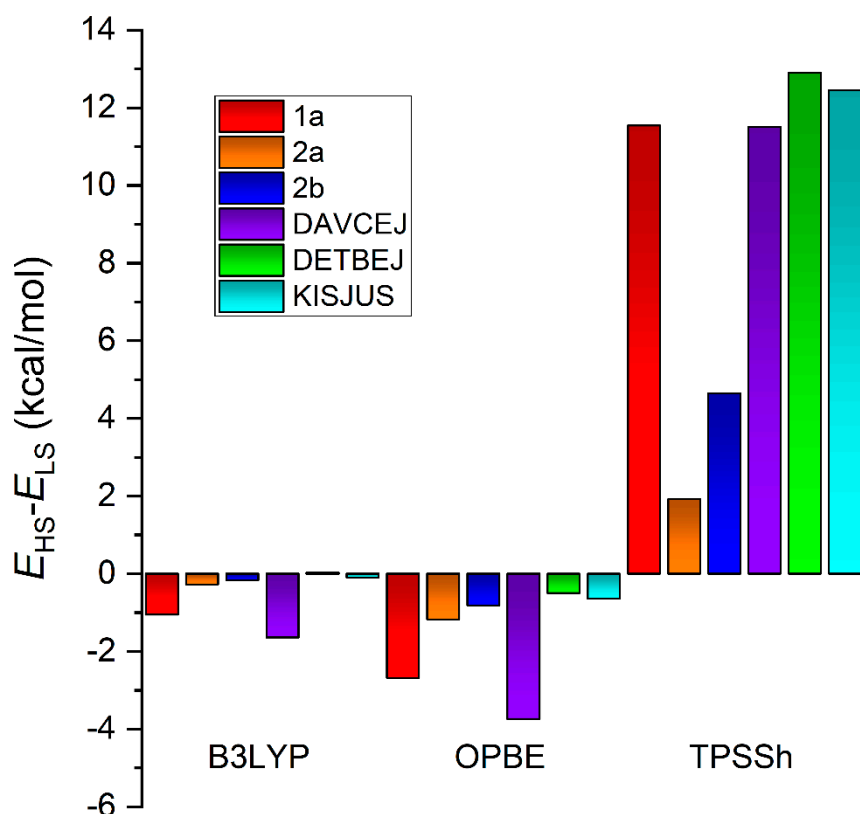


**Figure 4.** The energy separation of HS and LS states of **1a**, **2a**, and **2b** and DAVCEJ, DETBEJ, and KISJUS calculated using B3LYP, OPBE, and TPSSh with the def2-TZVP basis set.

#### 4. Conclusions

In this article we reported the synthesis, crystal structure, and magnetic properties of three new iron(III) complexes with two different pentadentate Schiff base ligands and monodentate heterocyclic ligands. The main motivation for this research was to increase the rather low cooperativity of

spin crossover behavior which was typically observed for this group of compounds previously. In general, it is well established that by introducing stacking interactions, the cooperativity of SCO systems might be enhanced. Therefore, relatively large, rigid, monodentate ligands (benzimidazole or 1-benzofuro[3,2-c]pyridine) capable of forming stacking interactions were deliberately introduced into the synthesis of the reported compounds. However, the prepared compounds did not exhibit any regular patterns of significant stacking interactions. The magnetic properties of the compounds showed that our attempt to increase SCO cooperativity was not successful, and the compounds exhibited weakly cooperative SCO without thermal hysteresis but with rather high critical SCO temperatures ( $T_{1/2} = 262$  (**1a**), 239 (**2a**), 365 (**2b**) K). DFT calculations were also employed in the study using three functionals, B3LYP, OPBE, and TPSSh. The best agreement with the experimental structures was found for the TPSSh functional, and also, only this functional identified LS isomers lower in energy than HS isomers. However, the general trend in the energy separation of HS and LS isomers and the spin crossover transition temperature  $T_{1/2}$  found from the experimental data was not fully recovered, which most probably points to the importance of the intermolecular interactions.

**Supplementary Materials:** The following are available online at <http://www.mdpi.com/2075-4701/9/8/849/s1>, Figure S1: The N–H... $\pi$  non-covalent interactions in **1a**, Figure S2: The non-covalent interactions in **2a**, Figure S3: The non-covalent interactions in **2b**, Table S1: The interatomic donor–acceptor distances for DFT-optimized geometries, Table S2: The interatomic donor–acceptor distances for DFT-optimized geometries.

**Author Contributions:** Conceptualization, I.N.; methodology, I.N. and R.H.; validation, I.N. and R.H.; formal analysis, R.H.; investigation, I.N., R.H. and I.S.; writing—original draft preparation, I.N. and R.H.; writing—review and editing, I.N. and R.H.; visualization, I.N. and R.H.

**Funding:** This research was funded by the institutional sources of the Department of Inorganic Chemistry, Palacký University Olomouc, Czech Republic (I.N. and R.H.), project CEITEC 2020 (LQ1601) with financial support from the Ministry of Education, Youth and Sports of the Czech Republic under the National Sustainability (I.N.).

**Acknowledgments:** Ivan Nemeč would like to acknowledge Jozef Miklovič for providing a small amount of 1-benzofuro[3,2-c]pyridine.

**Conflicts of Interest:** The authors declare no conflict of interest.

## References

1. Van Koningsbruggen, P.J.; Maeda, Y.; Oshio, H. Iron(III) spin crossover compounds. In *Spin Crossover in Transition Metal Compounds I*; Gülich, P., Goodwin, H.A., Eds.; Springer: Berlin, Germany, 2004; pp. 259–324.
2. Harding, D.J.; Harding, P.; Phonsri, W. Spin crossover in iron(III) complexes. *Coord. Chem. Rev.* **2016**, *313*, 38–61. [[CrossRef](#)]
3. Nemeč, I.; Boča, R.; Herchel, R.; Trávníček, Z.; Gembický, M.; Linert, W. Dinuclear Fe(III) complexes with spin crossover. *Monatshfte Chem. Chem. Mon.* **2009**, *140*, 815–828. [[CrossRef](#)]
4. Herchel, R.; Boča, R.; Gembický, M.; Kožíšek, J.; Renz, F. Spin Crossover in a Tetranuclear Cr(III)–Fe(III)<sub>3</sub> Complex. *Inorg. Chem.* **2004**, *43*, 4103–4105. [[CrossRef](#)] [[PubMed](#)]
5. Nemeč, I.; Herchel, R.; Boča, R.; Trávníček, Z.; Svoboda, I.; Fuess, H.; Linert, W. Tuning of spin crossover behaviour in iron(III) complexes involving pentadentate Schiff bases and pseudohalides. *Dalton Trans.* **2011**, *40*, 10090–10099. [[CrossRef](#)] [[PubMed](#)]
6. Nemeč, I.; Herchel, R.; Trávníček, Z. The relationship between the strength of hydrogen bonding and spin crossover behaviour in a series of iron(III) Schiff base complexes. *Dalton Trans.* **2015**, *44*, 4474–4484. [[CrossRef](#)] [[PubMed](#)]
7. Pogány, L.; Brachňáková, B.; Moncol, J.; Pavlik, J.; Nemeč, I.; Trávníček, Z.; Mazúr, M.; Bučinský, L.; Suchánek, L.; Šalitraš, I. Impact of substituent variation on the presence of thermal spin crossover in a series of mononuclear iron(III) schiff base complexes with terminal pseudohalido co-ligands. *Chem. A Eur. J.* **2018**, *24*, 5191–5203. [[CrossRef](#)] [[PubMed](#)]
8. Matsumoto, N.; Ohta, S.; Yoshimura, C.; Ohyoshi, A.; Kohata, S.; Okawa, H.; Maeda, Y. Studies on spin-equilibrium iron(III) complexes. Part 1. Syntheses and magnetic properties of a new family of spin cross-over iron(III) complexes with a unidentate ligand over a wide range of the spectrochemical series and a quinquedentate ligand derived. *J. Chem. Soc. Dalt. Trans.* **1985**, *12*, 2575. [[CrossRef](#)]

9. Boča, R.; Fukuda, Y.; Gembický, M.; Herchel, R.; Jaroščiak, R.; Linert, W.; Renz, F.; Yuzurihara, J. Spin crossover in mononuclear and binuclear iron(III) complexes with pentadentate Schiff-base ligands. *Chem. Phys. Lett.* **2000**, *325*, 411–419. [[CrossRef](#)]
10. Tanimura, K.; Kitashima, R.; Bréfuel, N.; Nakamura, M.; Matsumoto, N.; Shova, S.; Tuchagues, J.-P. Infinite chain structure and steep spin crossover of a Fe III Complex with a N<sub>3</sub>O<sub>2</sub> pentadentate schiff-base ligand and 4-aminopyridine. *Bull. Chem. Soc. Jpn.* **2005**, *78*, 1279–1282. [[CrossRef](#)]
11. Faulmann, C.; Dorbes, S.; De Bonneval, B.G.; Molnár, G.; Bousseksou, A.; Gomez-Garcia, C.J.; Coronado, E.; Valade, L. Towards molecular conductors with a spin-crossover phenomenon: Crystal structures, magnetic properties and Mössbauer spectra of [Fe(salten)mepepy][M(dmit)<sub>2</sub>] complexes. *Eur. J. Inorg. Chem.* **2005**, 3261–3270. [[CrossRef](#)]
12. Bannwarth, A.; Schmidt, S.O.; Peters, G.; Sönnichsen, F.D.; Thimm, W.; Herges, R.; Tuczek, F. feiii spin-crossover complexes with photoisomerizable ligands: Experimental and theoretical studies on the ligand-driven light-induced spin change effect. *Eur. J. Inorg. Chem.* **2012**, *2012*, 2776–2783. [[CrossRef](#)]
13. Bobošík, V.; Krutošíková, A.; Jordis, U. Synthesis and reactions of 2,3-dimethylfuro[3,2-c]pyridines. *Monatshefte für Chemie Chem. Mon* **1995**, *126*, 747–752. [[CrossRef](#)]
14. Bencková, M.; Krutošíková, A. Synthesis of pyrrolo[2',3':4,5]furo[3,2-c]pyridines. *Monatshefte Chem. Chem. Mon.* **1995**, *126*, 753–758. [[CrossRef](#)]
15. Sheldrick, G.M. Crystal structure refinement with SHELXL. *Acta Crystallogr. Sect. C Struct. Chem.* **2015**, *71*, 3–8. [[CrossRef](#)]
16. Neese, F. Software update: The ORCA program system, version 4.0. *Wiley Interdiscip. Rev. Comput. Mol. Sci.* **2018**, *8*, e1327. [[CrossRef](#)]
17. Becke, A.D. Density-functional exchange-energy approximation with correct asymptotic behavior. *Phys. Rev. A* **1988**, *38*, 3098–3100. [[CrossRef](#)]
18. Lee, C.; Yang, W.; Parr, R.G. Development of the Colle-Salvetti correlation-energy formula into a functional of the electron density. *Phys. Rev. B* **1988**, *37*, 785–789. [[CrossRef](#)]
19. Stephens, P.J.; Devlin, F.J.; Chabalowski, C.F.; Frisch, M.J. Ab Initio calculation of vibrational absorption and circular dichroism spectra using density functional force fields. *J. Phys. Chem.* **1994**, *98*, 11623–11627. [[CrossRef](#)]
20. Handy, N.C.; Cohen, A.J. Left-right correlation energy. *Mol. Phys.* **2001**, *99*, 403–412. [[CrossRef](#)]
21. Perdew, J.P.; Burke, K.; Ernzerhof, M. Generalized gradient approximation made simple. *Phys. Rev. Lett.* **1996**, *77*, 3865–3868. [[CrossRef](#)]
22. Perdew, J.P.; Kurth, S.; Zupan, A.; Blaha, P. Accurate density functional with correct formal properties: A step beyond the generalized gradient approximation. *Phys. Rev. Lett.* **1999**, *82*, 2544–2547. [[CrossRef](#)]
23. Perdew, J.P.; Tao, J.; Staroverov, V.N.; Scuseria, G.E. Meta-generalized gradient approximation: Explanation of a realistic nonempirical density functional. *J. Chem. Phys.* **2004**, *120*, 6898–6911. [[CrossRef](#)] [[PubMed](#)]
24. Weigend, F.; Ahlrichs, R. Balanced basis sets of split valence, triple zeta valence and quadruple zeta valence quality for H to Rn: Design and assessment of accuracy. *Phys. Chem. Chem. Phys.* **2005**, *7*, 3297–3305. [[CrossRef](#)]
25. Weigend, F. Accurate Coulomb-fitting basis sets for H to Rn. *Phys. Chem. Chem. Phys.* **2006**, *8*, 1057–1065. [[CrossRef](#)] [[PubMed](#)]
26. Neese, F.; Wennmohs, F.; Hansen, A.; Becker, U. Efficient, approximate and parallel Hartree-Fock and hybrid DFT calculations. A “chain-of-spheres” algorithm for the Hartree-Fock exchange. *Chem. Phys.* **2009**, *356*, 98–109. [[CrossRef](#)]
27. Izsák, R.; Neese, F. An overlap fitted chain of spheres exchange method. *J. Chem. Phys.* **2011**, *135*, 144105. [[CrossRef](#)] [[PubMed](#)]
28. Seeger, R.; Pople, J.A. Self-consistent Molecular Orbital Methods. XVIII. Constraints and Stability in Hartree-Fock Theory. *J. Chem. Phys.* **1977**, *66*, 3045–3050. [[CrossRef](#)]
29. Bauernschmitt, R.; Ahlrichs, R. Stability Analysis for Solutions of the Closed Shell Kohn-Sham Equation. *J. Chem. Phys.* **1996**, *104*, 9047–9052. [[CrossRef](#)]
30. Spek, A.L. Platon Squeeze: A tool for the calculation of the disordered solvent contribution to the calculated structure factors. *Acta Crystallogr. Sect. C Struct. Chem.* **2015**, *71*, 9–18. [[CrossRef](#)] [[PubMed](#)]
31. Nemeč, I.; Boča, R.; Gembický, M.; Dlháň, L.; Herchel, R.; Renz, F. High-spin Schiff-base dinuclear iron(III) complexes bridged by N-oxide ligands. *Inorg. Chim. Acta* **2009**, *362*, 4754–4759. [[CrossRef](#)]

32. Guionneau, P.; Marchivie, M.; Bravic, G.; Letard, J.F.; Chasseau, D. Structural aspects of spin crossover. Example of the [(FeLn)-L-II(NCS)(2)] complexes. *Top. Curr. Chem.* **2004**, *234*, 97.
33. Bari, R.A.; Sivadrière, J. Low-spin-high-spin transitions in transition-metal-ion compounds. *Phys. Rev. B* **1972**, *5*, 4466–4471. [[CrossRef](#)]
34. Wajnflasz, J. Etude de la transition “Low Spin”-„High Spin” dans les complexes octaédriques d’ion de transition. *Phys. Status Solidi* **1970**, *40*, 537–545. [[CrossRef](#)]
35. Boča, R.; Linert, W. Is There a Need for New Models of the Spin Crossover? *Monatshefte Chem. Chem. Mon.* **2003**, *134*, 199–216. [[CrossRef](#)]
36. Siig, O.S.; Kepp, K.P. Iron(II) and Iron(III) spin crossover: Toward an optimal density functional. *J. Phys. Chem. A* **2018**, *122*, 4208–4217. [[CrossRef](#)] [[PubMed](#)]
37. Cirera, J.; Via-Nadal, M.; Ruiz, E. Benchmarking density functional methods for calculation of state energies of first row spin-crossover molecules. *Inorg. Chem.* **2018**, *57*, 14097–14105. [[CrossRef](#)] [[PubMed](#)]
38. Swart, M.; Groenhof, A.R.; Ehlers, A.W.; Lammertsma, K. Validation of exchange–correlation functionals for spin states of iron complexes. *J. Phys. Chem. A* **2004**, *108*, 5479–5483. [[CrossRef](#)]



© 2019 by the authors. Licensee MDPI, Basel, Switzerland. This article is an open access article distributed under the terms and conditions of the Creative Commons Attribution (CC BY) license (<http://creativecommons.org/licenses/by/4.0/>).